

Investigations on servicing damage mechanisms of Cr35Ni45Nb alloy under complex conditions

Jiangchu Xiao^{b)} and Maicang Zhang^{a)}

School of Material science and engineering, University of Science & Technology Beijing, Beijing 100083, China

(Received 8 October 2015; accepted 11 April 2016)

The damage induced by oxidation and stress during the service process of Cr35Ni45Nb alloy and their influences on the microstructure evolution and creep rupture life of this alloy were studied. Continuity, compactness, and high temperature stability of the oxide layers are conducive to the performance of the alloy. A slight but complete layer of oxidation on surface improves the creep rupture life of the specimens. However, being exposed to long-term oxidation is observed to be counter-productive. Temperature stress generated during the air-cooling process creates large carbides near the surface of the specimen's cracks. Moreover, tiny carbides are precipitated from γ matrix and interfacial defects due to creep stress, but strip carbides are dissolved due to creep stress and the Gibbs–Thomson effect.

I. INTRODUCTION

Ethylene cracking furnace tube is a core component in petrochemical plants. Cracking furnace tubes are operated under stress for a long term in the complex condition like high temperature, oxidation, and carburization. As austenitic heat resistant steel is capable of withstanding high temperature and has good properties of antioxidation and carburization, it becomes the first choice.^{1,2} Cr35Ni45Nb alloy is widely used for manufacturing ethylene cracking furnace tubes due to its excellent mechanical and anticorrosion performances. The cracking furnace tubes are easy to be damaged while being exposed in an environment of oxidation and carburizing for a long time.³ Besides, the presence of thermal stress is one of the main reasons for creep failure of the tubes during long-term services. Industrial observation has shown that surface oxides of cracking tubes are widespread in the process of servicing.^{4,5} Under most industrial conditions, protection against carburization and catalytic coke formation is provided by means of an oxide layer and several studies have focused on the formation of such protective oxide layers during in situ or preoxidation.^{6–8} These layers are strong barriers against diffusion of carbon.⁵ However, the fundamental problem is that those protective oxide layers show little thermal stability.⁹ Furthermore, with the formation of the oxide layer, diffusion of elements like chromium onto the surface for forming chromium oxides leads to the depletion of carbide within subsurface regions of the alloy.¹⁰

The loss of carbides on the grain boundary would weaken the mechanical properties of the alloy such as strength, plasticity, and thermal expansion coefficient, leading to the decrease of the creep resistance of the grain boundary during high temperature service, which may in turn cause catastrophic fractures of the tubes.¹¹

In general, ethylene cracking furnace tube is operated under the temperature between 900 and 1100 °C or higher than 1100 °C and the stress of no more than 2 MPa.^{12,13} During its operating process, the outer wall of the furnace tube is heated by flame radiation, then the heat is transferred into the inner wall by heat conduction. Thus, a temperature difference is generated between the inner and outer walls, resulting in thermal stress in radial direction of the tube. By now, little investigations consider the comprehensive effects of oxidation and thermal stress for ethylene cracking furnace tubes during their servicing process. It has important reference value on the engineering of the concrete corrosion protection measures of the alloy and alloy modification to study the oxidation and stress damage mechanism of Cr45Ni45Nb alloy. The present work focuses on the microstructure transformation and its influence on the creep rupture life of Cr35Ni45Nb tubes under different pretreatment or test conditions, to study the micro-damage mechanisms for this tube components.

II. EXPERIMENTAL PROCEDURES

A Cr35Ni45Nb tube, serviced for 2.5 years, was divided into three parts for different further treatments. The specimens of 3 mm in diameter of the alloy for high temperature creep rupture tests are cut from the heat treated tubes. The chemical components of the alloy are listed in Table I.

Contributing Editor: Jürgen Eckert

Address all correspondence to these authors.

^{a)}e-mail: mczhang@ustb.edu.cn

^{b)}e-mail: Gemini_xiao@163.com

DOI: 10.1557/jmr.2016.175

TABLE I. The chemical compositions of Cr35Ni45Nb alloy.

Elements	C	Nb	Cr	Si	O	Ni	Fe
wt%	0.45	1.20	35.44	1.64	0.82	42.68	Bal.

To study the effect of stress on the microstructure and creep rupture life of Cr35Ni45Nb alloy, 3 specimens were sent to high temperature creep rupture tests at 1080 °C under the stress of 10, 15, and 25 MPa, using UHRD304-B1 tester (Shenzhen Sansi Instrument and Equipment Co., Ltd., Shenzhen, China). To further study the microstructure evolution during the process of oxidation and its effects on the creep rupture life of the alloy, 2 specimens were heat-treated at 1080 °C for 50 and 350 h (the same as the creep rupture life of some specimens tested before) under laboratory conditions using SRJX-4-13 box resistance furnace (Nanjing Xiaoxiao Instrument and Equipment Co., Ltd., Nanjing, China) before creep rupture tests. A specimen which had not been preoxidized was also tested as a comparison. The specimens after different pretreatments were sent to high temperature creep rupture tests at 1080 °C under the stress of 15 MPa.

After preoxidation, and creep rupture life tests, phase composition analysis and microstructure analysis were conducted on metallographic specimens which had been cut from the proceeding specimens along the axis. The specimens after tests were mechanically grinded, polished, and etched with a solution mixed of 80 ml concentrated hydrochloric acid and 8 g oxalic acid. Then, the microstructures and phase composition of the specimens were analyzed with JSM-6510A scanning electron microscope (Japan Electron Optics Laboratory Co. Ltd., Japan) equipped with a JED-2300 energy dispersive spectrometer (Japan Electron Optics Laboratory Co. Ltd., Japan) at 10 kV. After that, quantitative analyses of the microstructure composition were carried out by a JXA-8230 electron probe micro-analyzer (EPMA; Japan Electron Optics Laboratory Co. Ltd., Japan) operated at 20 kV.

III. RESULTS AND DISCUSSIONS

A. Microstructure evolution of preoxidized specimens after creep rupture tests

The microstructures of the specimens after different pretreatment are shown in Fig. 1. The surface layer of the tube is composed of 3 well-defined zones including composite oxide layer, carbide depleted zone, and inner normal region. The composite oxide layers distributing on the surface are of different thickness. It can be divided into 2 parts, the outer continuous oxide layer and the inner discontinuous granular-oxide layer. The chemical components of the oxide layers are listed in Table II. According to the EPMA quantitative chemical analysis, the outer

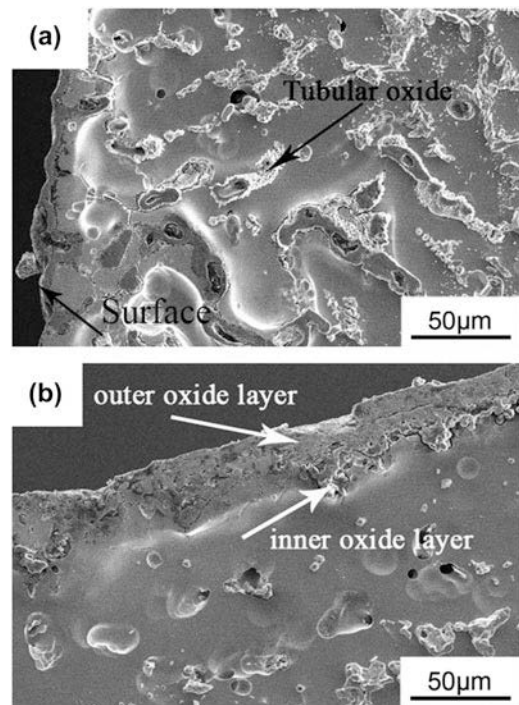


FIG. 1. Microstructure of specimens after different pretreatment: (a) untreated specimens (b) preoxidation treated for 50 h.

TABLE II. EPMA analysis results of the oxide component (a) inner oxide, (b) outer oxide.

Element	C	O	Si	Ni	Cr	Nb	Fe
Atom a	16.9379	53.9983	25.1615	0.6975	2.8983	0.0362	0.2704
(%) b	0	67.1653	0.0113	0.2843	32.4173	0.0122	0.1097

thicker oxide layer is mainly consisted of Cr_2O_3 , and the inner layer is SiO_2 . As the phase of Fig. 1(a) is small, C elements in the matrix are more easily detected.

Compared with the specimen that has been preoxidation treated for 50 h [Fig. 1(b)], the carbide depleted zone in untreated specimen [Fig. 1(a)] is covered with large size oxides. The oxides in the carbide depleted zone of untreated specimen have a tubular double-layer structure [Fig. 1(a)]; however, in the preoxidized specimen, the carbides are granular and seldom observed. The tubular oxide structure consists of two layers of oxide film. According to the EPMA quantitative chemical analysis, the inner layer is composed of Cr_2O_3 while the outer layer is mainly SiO_2 . The formation of this structure is closely related to the creep process of the materials and the affinity between alloy elements and oxygen.

Under the effect of high temperature and creep stress, cavities generated at the branch boundaries which are perpendicular to the stress axis¹⁴ because of grain boundary sliding. Then the cavities gathered to form a fast channel of gas along the branch boundaries, through which the outside oxidizing atmosphere was

able to enter the matrix and oxidize the structure surrounding the channel. According to the basic theory of material science, the oxidation of the elements and the formation of the oxide in the alloys are all dynamic and thermodynamic process. Under the same oxygen partial pressure, the priority of the formation of Cr_2O_3 and SiO_2 is related to their free energy of Gibbs formation (ΔG). According to the Ellingham oxygen potential figure,¹⁵ ΔG_{SiO_2} is lower than $\Delta G_{\text{Cr}_2\text{O}_3}$; in other words, the free energy of Gibbs formation of SiO_2 is lower than that of Cr_2O_3 . At the beginning of the formation of the oxide film, partial pressure of the oxygen diffusing to the interface is still high, and $\Delta G_{\text{Cr}_2\text{O}_3}$ is under 0. While Cr is of high concentration, it can form a single oxide layer; as a result, Cr is first oxidized to form the Cr_2O_3 oxide layer. With the thickening of the oxide layer, the diffusing of oxygen to the matrix becomes more difficult, thus the partial pressure of oxygen of the interface comes down. At that time $\Delta G_{\text{Cr}_2\text{O}_3} = 0$, and the Cr_2O_3 layer stops growing. Si, which has a stronger binding capacity toward oxygen, begins to form the granular silicon oxide near the Cr_2O_3 oxide layer.¹⁶ The tubular structure of Cr_2O_3 oxidation layer packaged with granular SiO_2 oxide outside is eventually formed.

The creep rupture time of specimens and their microstructure characteristics after different time-length of preoxidation are shown in Fig. 2. Specimens being preoxidized for 50 h have a longer creep rupture life, for its oxide layer has a better condition—few cracks are observed. The Cr_2O_3 oxide layer is of high bond strength. The crack which formed from the interface extends into the layer, and then causes the whole oxide layer to peel off. This rupture of the oxide layer follows the Evans rule.^{17,18} The cracked oxide layer stops working as a protector of the matrix; and the matrix is exposed directly to the oxidizing atmosphere and carburization environment. It is observed in long term preoxidized specimens that the oxide layer of the boundary peels off badly; the oxide layer subsequently formed is highly discontinuous; and lots of cavities have formed in the carbide depleted zone under the depth of about 95 μm right behind the oxide layer.

After a short-time (50 h) preoxidation treatment, a thin layer of oxide, which has a good performance of adhesion, formatted on the surface of the specimen. At this point, the cracking of the oxide layer demands high critical stress.¹⁹ The oxide layer, which plays a protective role to the alloy matrix to some extent, prevents the outside atmosphere from further oxidizing the alloy matrix. In fact, if the oxide layer on the surface is compact and closely combined with the matrix; in other words, if it does not crack or peel off during the servicing process, the oxide layer would improve the creep properties of the alloy.²⁰ Therefore, the specimen being preoxidized for 50 h has a longer creep rupture life than

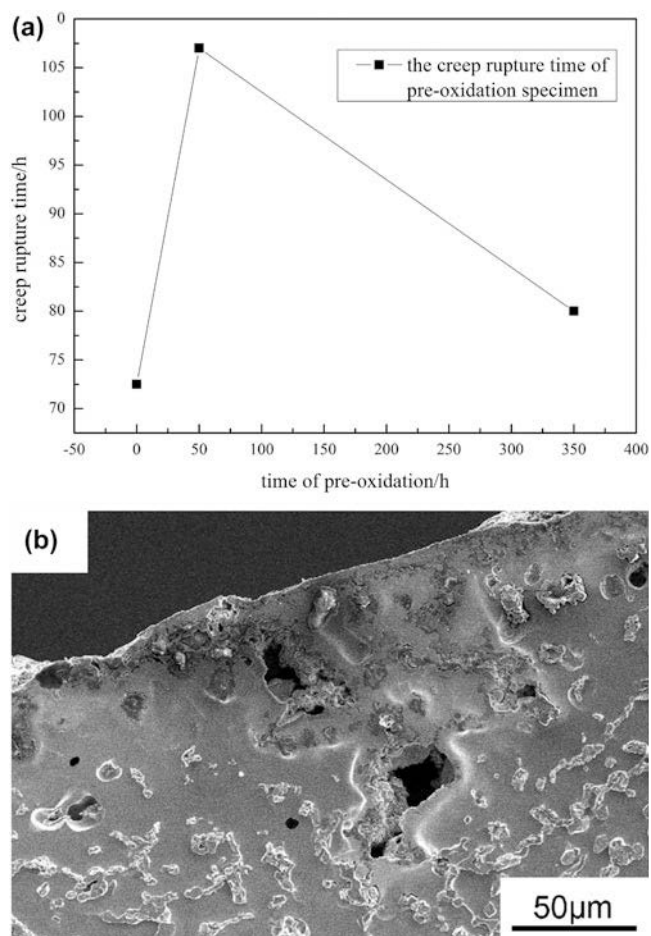


FIG. 2. Creep rupture life and the microstructure of preoxidized specimens: (a) creep rupture life of preoxidized specimens (b) preoxidized for 350 h.

those without pretreatment. However, after a longer time (350 h) of preoxidation, the oxide layer is no longer continuous and loses the ability to protect the internal matrix. The formation of internal oxidation in the grain boundary leads to the reduction of its strength. As a result, the grain boundary turns out to be a rapid expanding channel for the cracks.

Both the cracking of the oxidation film and the internal oxidative damage can result in the loss of the internal bearing area, leading to the loss of the bearing capacity of the specimen eventually. Set a damage variable D for oxidative damage area fraction, λ for the impact factor of internal oxidative damage. The damage differential equation is given by Eq. (1) as follows²¹:

$$dD = \frac{2}{r} \left[\frac{\lambda c_1}{rD} + (1 - \lambda) \left(\frac{2c_p \dot{\epsilon}}{\epsilon_M} \right)^{1/2} \right] dt \quad (1)$$

in which, r is the radius of the specimen, $\dot{\epsilon}$ is the creep rate, ϵ_M refers to the strain of oxide layer cracking, and c_1 , c_p are both kinetic constants. The first part of the

differential equation refers to the internal oxidative damage, and the other refers to the crack damage of oxide layer. When the effective bearing area is reduced to zero, the specimen will crack. To integrate the equation, Eq. (2) can be obtained:

$$t_1 = \frac{\lambda D_1^2 r^2}{4c_1} + \frac{(1-\lambda)r}{n+2} \left(\frac{\varepsilon_M}{2c_p \dot{\varepsilon}_M} \right)^{1/2} \left[1 - (1 - D_1)^{n/2} \right] \quad (2)$$

in which, n is the stress index of the steady creep rate, and D_1 is the critical damage value of Cr35Ni45Nb alloy.

Under the effect of stress and thermal shock, the oxide layer may easily crack. Once the oxide layer cracks, it loses its bearing capacity. Even though it is healed afterward, the effective bearing area of the alloy still decreases. In the process of this kind of craze-healing cycle, the alloy's creep rupture life is reduced.

Moreover, severe oxidation on the boundary causes the widespread formation of the carbide depleted zone. The carbide depleted zone will weaken the properties of the alloy, leading to the nonuniform performance (such as strength, plasticity, thermal expansion coefficient, etc.) of the tube along the radial direction.²² The grain boundary in the carbide depleted zone is of poor creep resistance performance, then the micro cracks initiating from the boundary expand rapidly within the zone due to the lack of carbide barriers. As a result, after long-term preoxidation, the creep rupture life of the specimen is reduced instead.

B. Influence of stress on carbide morphology

1. Influence of temperature stress on carbide morphology

Within 150 μm to the surface of the specimen, M_7C_3 , the primary carbides whose sizes are beyond 10 μm , crack during air-cooling after high temperature aging (Fig. 3). Some of the carbides peeled off directly from the matrix, leaving a large cavity.

During air-cooling, the room temperature is around 25 $^\circ\text{C}$, while the initial temperature of the specimen is

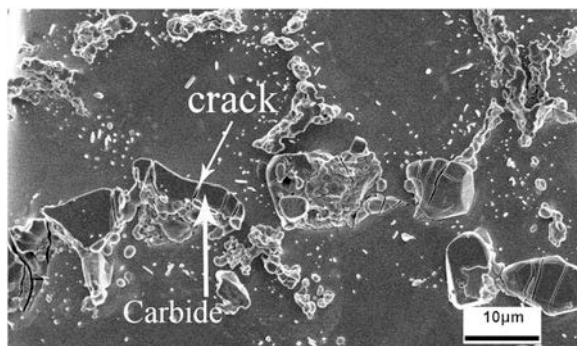


FIG. 3. Carbide morphology characteristics near the boundary.

1080 $^\circ\text{C}$. This great difference in temperature makes the outmost layer of the specimens, which is exposed directly to the air, cool down rapidly. Because of the obvious difference of thermal expansion coefficient and thermal conductivity between the carbides and the matrix, when the matrix contracts drastically during the process of air-cooling, a great deal of stress generates on the carbide–matrix interface, which results in the plastic deformation of the matrix around the carbides. The expansion coefficient of the carbides is less than that of the γ matrix, thus the compressive stress generates in the process of air cooling. The compressive stress σ_r on the radial direction can be expressed as:²³

$$\sigma_r = -2Y \left[\ln \frac{R'}{r} + \frac{1}{3} (1 - h^3) \right] \quad (3)$$

in which, Y is the yield strength of γ matrix; R' is the radius of plastic deformation zone caused by internal stress, and R' is associated with $(\alpha - \alpha_i)$ and ΔT ; r is the distance of any point in the plastic deformation area to the center of the carbide; h is the ratio of the distance between plastic deformation area and the midpoints of two adjacent carbides.

$(\alpha - \alpha_i)\Delta T$ refers to thermal stress potential,²⁴ which directly decides the value of internal stress. The greater the difference of thermal expansion coefficient $(\alpha - \alpha_i)$ between the matrix and the carbides is, the larger the plastic deformation zone is, and the greater the stress generates in the process of air-cooling.

Under the stress, carbides of jumbo size crack, some of which even peeling off directly from the matrix. Cavities are likely to form between the carbide and the matrix after the cracking, becoming another potential source of cracks. Besides, after the cracking, carbides tend to have sharp boundaries where stress concentration frequently happens, which in turn results in the dissolution of the carbides.

In actual service conditions, the furnace tube needs regular maintenance and decoking. The operation and stop of the cracking plant causes thermal shock to the furnace tube, producing temperature stress within a certain thickness range of the inner and outer wall of the furnace tube. The cracking of large carbides on the surface of the furnace due to temperature stress is very likely to generate crack initiation and expansion. As a result, service life of the furnace tube is badly affected.

2. Influence of applied stress on carbide morphology

Figure 4 shows the microstructure of specimens after direct aging or creep rupture life tests. After direct aging, carbides present a shape of long strip; the longest one can reach 100 μm . Several carbides gather into clumps; some

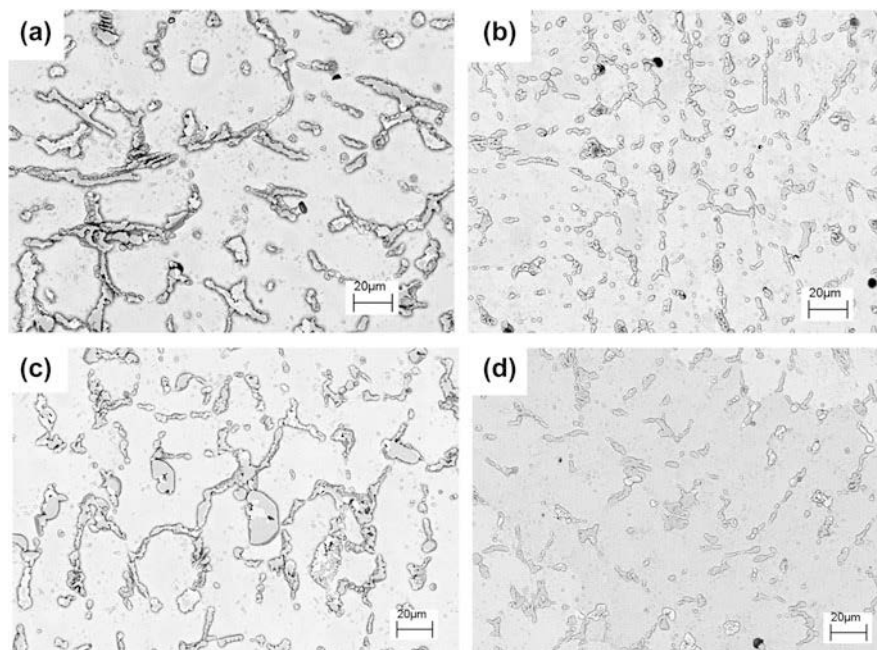


FIG. 4. Microstructure of specimens after aging and creep rupture life tests: (a) aging for 5 h (b) creep rupture life test for 5 h (c) aging for 72 h (d) creep rupture life test for 72 h.

present discontinuous reticular structure; and there are a number of small granular carbides precipitate from the γ matrix. However, after creep rupture test, most of the carbides are podgy, smooth, and independent as small granules. With the extension of time, the carbides in both specimens get coarsened, and the number of carbides decreases significantly. In matrix of the specimens after short-time aging, many tiny granular carbides distribute around the primary carbides. As the aging gets longer, the number of tiny granular carbides decreases gradually, and they begin to distribute along the interdendritic instead of dispersedly in the matrix.

In the creep rupture life test, a small quantity of tiny granular carbides disperse in the matrix of short life specimens. As the test gets longer, the primary carbides of large size coalesce to grow, with more tiny carbides dispersing in the matrix.

With the extension of aging time, tiny carbides in the specimens kept decreasing; however, in the creep rupture life tests, tiny carbides in the specimens increased instead. It shows that stress is beneficial to the precipitation of tiny carbides. Applied stress makes the material distorted. To reduce the system energy, carbon atoms migrate from matrix to grain boundary, phase boundary, and dislocation defect zone. Besides, the defect in crystal also acts as a fast channel for the elements to diffuse providing a favorable condition for the formation of the rich solute core as well as the segregation of carbon at defect zone, which in turn makes possible the precipitation of tiny carbides in the matrix.

In addition, applied stress will change the solubility of elements in γ matrix. According to the theory of thermodynamics about the influence of stress on the phase equilibrium,²⁵ coupled with the rule solution model,²⁶ according to the Ref. 27, the relationship between applied stress and the solubility of C elements in γ matrix is modified as the following equation:

$$\ln\left(\frac{X_C}{X_C^0}\right) = \frac{\sigma V}{RTX_C} \quad (4)$$

in which, X_C^0 and X_C is the mole fraction that element C dissolving in γ matrix without stress and in the condition of stress; σ is applied stress; R is gas constant; T is thermodynamic temperature, and V is the molar volume of carbides. The ratio of the solubility of C under stress to its solubility without stress presents a logarithmic relationship with stress. When the stress is tensile, σ turns out to be negative, and $\left(\frac{X_C}{X_C^0}\right) < 1$, indicating that in creep rupture life tests under low stress, the solubility of C in γ matrix decreases due to the effect of tensile stress.

During the creep rupture life test, the creep deformation of specimens under stress causes dislocation accumulation and the rise of energy of distortion. To reduce the energy of the system, tensile stress is added to reduce the solubility of C in the matrix, thus C elements aggregate to the defect. The increasing of the concentration of C in the defect results in the precipitation of tiny carbides of C element in the matrix and the flaw interface.

Since the strip carbides are able to hinder the dislocation movement effectively, stress concentration can be easily produced in the process of creep rupture life test. Then subsidiary stress is formed on the surface of the strip carbides. According to the Ref. 27, the relationship between the concentration of C in the matrix and subsidiary stress is shown in the following equation:

$$X_C^\gamma = {}^0X_C^\gamma \exp\left(\frac{PV}{RTX_C}\right) \quad (5)$$

in which, X_C^γ and X_C are respectively the mole concentration of C element in the matrix and the carbide; V is the molar volume of the carbide; ${}^0X_C^\gamma$ is the molar concentration of C element in the matrix under unstressed condition; P is the subsidiary stress. During the creep rupture life test, the deformation of the matrix increases, and the subsidiary stress on the surface of the strip carbide also increases, resulting in the increase of solubility of C element in the adjacent γ matrix. Then, C element in the carbides naturally diffuses into γ matrix, which accelerates the dissociation of the carbides.

In fact, continuous interdendritic carbide is not a complete strip; instead, it is lapped by lots of equiaxial granular carbides of regular geometry shape (Fig. 5a). The carbide has its own interface; under low stress, there is strong bonding force between the carbide particles, which makes it hard to crack. However, in this kind of lap structure there is inevitably weak links where the bonding easily becomes flexible under the creep stress. Due to the effect of subsidiary stress, these weak positions gradually break down to form grooves, thus the radius of curvature of the carbides in these positions are smaller than that of others.²⁸ Similar to the mechanism of particle coarsening, the Gibbs–Thomson effect (the phenomenon that

saturation concentration increases with the radius of curvature in solid state transformation²⁹) generated on the grooves, which produces concentration gradient. The mathematics analytic expression is given by Eq. (6) as follows,

$$C_r^\alpha = C_\infty^\alpha \left[1 + \frac{2\sigma V}{RT} \frac{1}{r} \right] \quad (6)$$

where, C_r^α is the saturation concentration when the radius of curvature is infinite; r is radius of curvature. Concentration gradient generated due to the Gibbs–Thomson effect, making C element in the grooves of the carbides diffuse to the matrix. To maintain the concentration balance, the carbides gradually dissolved, thus the curvature became larger, and the interfacial tension generating between the groove and the adjacent matrix increased as well. According to the Ref. 29, the instantaneous balance relationship between the subsidiary stress P and the interfacial tension between the γ matrix and the carbides on both sides of the groove is given by Eq. (7) as follows,

$$P = 2\sigma \cos \frac{\alpha}{2} \quad (7)$$

in which, σ is the interfacial tension between the groove formed with the resolving of the carbide and adjacent γ matrix; α is the angle formed by resolved carbides [Fig. 5(b)]. In the process of creep, cracks and cavities appeared in some parts, and then the local stress increased, which in turn resulted in the increasing of subsidiary stress on the surface of strip carbides. With the increasing of local applied stress, the tension at the intersection of the groove got out of balance. To maintain the balance, the carbides on the surface of the groove

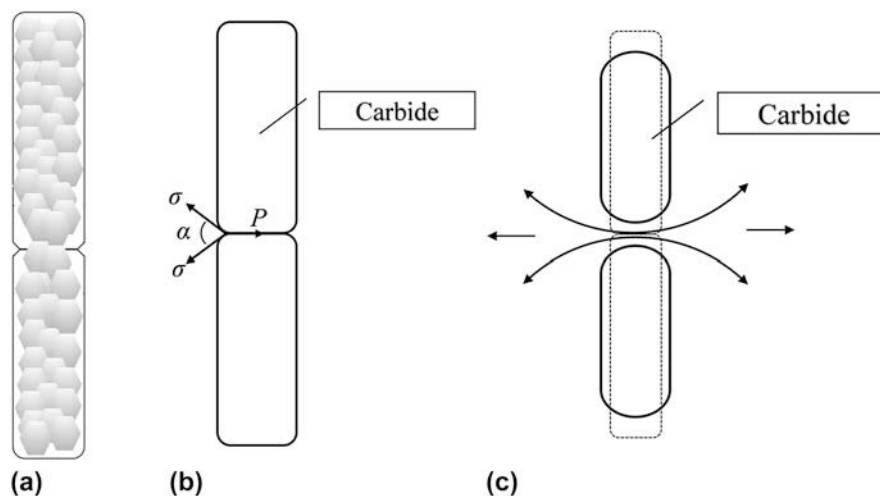


FIG. 5. The evolution of strip carbide: (a) the lap structure of strip carbides (b) stress moment balance on groove (c) strip carbide dissolved into two pieces of small carbides.

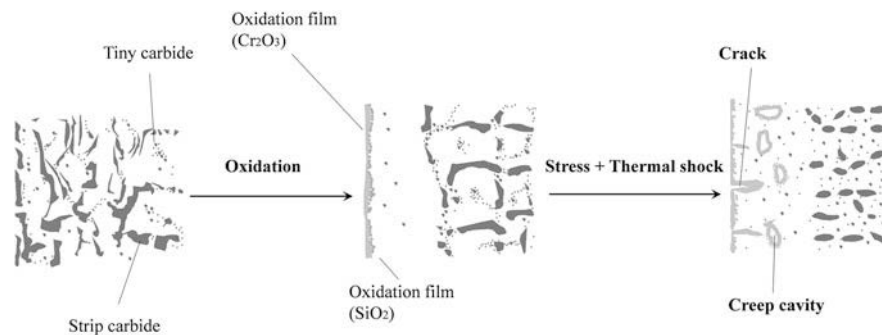


FIG. 6. Microstructure evolution in different conditions.

dissolved, forming two pieces of small carbides eventually [Fig. 5(c)].

In conclusion, the subsidiary stress generating on the surface of the strip carbide results in the appearance of grooves in weak points. Under the effect of subsidiary stress and Gibbs–Thomson effect, the groove gradually deepened, which leads to the dissolution of the carbide on the groove. As a result, the carbides in the specimens after creep rupture tests appear to be small, and without sharp edges.

In the original structure of the specimens which have serviced for 2.5a, tiny granular carbides precipitated around the strip carbides, forming a discontinuous net structure. After high temperature oxidation, microstructure of the specimens were changed, oxidation film as well as the carbide depleted zone were formed, and the inner carbides decreased in number. Under the action of high temperature oxidation, stress and thermal shock, etc., the oxidation film on the boundary fractures, then cracks formed. Creep cavities formed in the carbide depleted zone. Strip carbides in the matrix dissolved to form smaller carbides, while tiny carbides precipitated from the matrix (refer to Fig. 6).

IV. CONCLUSION

(1) The Cr_2O_3 and SiO_2 layers cooperate to prevent the infiltration of the carbon and further oxidation of the inner matrix. To some extent, slight oxidation on the surface can increase the creep rupture life of specimens. However, in long term service, a long creep rupture life of the specimen requires continuity, compactness, and high temperature stability of the oxide layers, which are hard to be met at the same time. One failure in the fulfillment of the three requirements, the oxidation would be harmful to the creep rupture life of the specimen. In long term service, several of stresses and thermal shock leading to the oxide layer crack, make the creep rupture life of the specimen reduce.

(2) During the process of cooling, there is a great difference in temperature between air and the interface of the specimen. The temperature stress generating between

the carbides and the matrix on the surface of the specimens because of the difference of thermal expansion coefficient between the carbide and γ matrix makes the large carbides crack. In the process of creep rupture life test, tiny carbides precipitated from γ matrix and the interface defect under the creep stress. However, under subsidiary stress and the Gibbs–Thomson effect, the strip carbides dissolved to form some small pieces of granular carbides.

ACKNOWLEDGMENT

This study was funded by National High-tech R&D Program-2012AA03A513. The authors are grateful for the financial support and facilities provided by China Special Equipment Inspection and Research Institute and Beijing Institute of Aeronautical Materials.

REFERENCES

1. S.H. Khodamorad, D. Haghshenas Fatmehsari, H. Rezaie, and A. Sadeghipour: Analysis of ethylene cracking furnace tubes. *Eng. Failure Anal.* **21**, 1 (2012).
2. A.A. Kaya, P. Krauklis, and D.J. Young: Microstructure of HK40 alloy after high temperature service in oxidizing/carburizing environment. *Mater. Charact.* **49**(1), 11 (2002).
3. H.J. Grabke and I. Wolf: Carburization and oxidation. *Mater. Sci. Eng.* **87**, 23 (1987).
4. Z. Zhu, C. Cheng, J. Zhao, and L. Wang: High temperature corrosion and microstructure deterioration of KHR35H radiant tubes in continuous annealing furnace. *Eng. Failure Anal.* **21**, 59 (2012).
5. S. Borjali, S.R. Allahkaram, and H. Khosravi: Effects of working temperature and carbon diffusion on the microstructure of high pressure heat-resistant stainless steel tubes used in pyrolysis furnaces during service condition. *Mater. Des.* **34**, 65 (2012).
6. A. Schnaas and H.J. Grabke: High-temperature corrosion and creep of Ni–Cr–Fe alloys in carburizing and oxidizing environments. *Oxid. Met.* **12**(5), 387 (1978).
7. H.J. Grabke, K. Ohla, J. Peters, and I. Wolf: Radiotracer studies of carbon permeation through oxide scales on commercial high temperature alloys and model alloys. *Mater. Corros.* **34**(10), 495 (1983).
8. T. Shinohara, I. Kohchi, K. Shibata, J. Sugitani, and K. Tsuchida: Development of nondestructive technique for measuring carburization thickness and of a new carburization-resistant alloy. *Mater. Corros.* **37**(7), 410 (1986).

9. C. Steurbaut, H.J. Grabke, D. Stobbe, F.R. Van Buren, S.J. Korf, and J. Defrancq: Kinetic studies of coke formation and removal on HP40 in cycled atmospheres at high temperatures. *Mater. Corros.* **49**(5), 352 (1998).
10. N. Xu, D. Monceau, D. Young, and J. Furtado: High temperature corrosion of cast heat resisting steels in CO + CO₂ gas mixtures. *Corros. Sci.* **50**(8), 2398 (2008).
11. S.K. Das, R.N. Ghosh, and S. Sondhi: Prediction of carbide free layer formation in Fe–Ni–Cr austenitic steel process heater tube. *Corros. Eng., Sci. Technol.* **47**(2), 121 (2012).
12. W.Z. Wang, F.Z. Xuan, Z.D. Wang, B. Wang, and C.J. Liu: Effect of overheating temperature on the microstructure and creep behavior of HP40Nb alloy. *Mater. Des.* **32**(7), 4010 (2011).
13. L.X. Li and F.R. Mao: Calculation of the carburization stress of the ethylene cracking furnace tubes. *Machinery Design & Manufacture* **47**(6), 42 (2009).
14. X.Z. Duan and Y.M. Zhang: The creep and corrosion behavior of M38G superalloy with ternary Al–Zr–Y coating. *J. Chin. Soc. Corrosion Protect.* **14**(1), 53 (1994).
15. K.X. Huang: *Iron and Steel Metallurgy Principle* (Metallurgical Industry Press, Beijing, 1990).
16. H. Wang, C.Y. Du, W. Li, Y.C. Peng, and M.C. Zhang: Research on behavior and mechanism of high temperature oxidation for Cr35Ni45Nb heat-resistant steel under servicing condition. *Hot Work. Technol.* **43**(18), 101 (2014).
17. L.H. de Almeida, A.F. Ribeiro, and I. Le May: Microstructural characterization of modified 25Cr–35Ni centrifugally cast steel furnace tubes. *Mater. Charact.* **49**(3), 219 (2002).
18. M. Mostafaï, M. Shamanian, H. Purmohamad, M. Amini, and A. Saatchi: Microstructural degradation of two cast heat resistant reformer tubes after long term service exposure. *Eng Fail Anal.* **18**(1), 164 (2011).
19. J. Robertson and M.I. Manning: Limits to adherence of oxide scales. *Mater. Sci. Technol.* **6**(1), 81 (1990).
20. R. Petkovic-Luton and T.A. Ramanarayanan: Mixed-oxidant attack of high-temperature alloys in carbon-and oxygen-containing environments. *Oxid. Met.* **34**(5–6), 381 (1990).
21. J.S. Zhang: *High Temperature Deformation and Fracture of Materials* (Science Press, Beijing, 2007).
22. X.Q. Wu, Y.S. Yang, Q. Zhan, and Z.Q. Hu: Structure degradation of HP cracking tube during service. *Acta Metall. Sin.* **34**, 1043 (1998).
23. T. Pan, Z.G. Zhang, B.Z. Bai, and H.S. Fang: Study of thermal stress and strain energy γ -Fe matrix around inclusion caused by thermal coefficient difference. *Acta Metall. Sin.* **39**(10), 1037 (2009).
24. D. Brooksbank and K.W. Andrews: Stress fields around inclusions and their relation to mechanical properties. *Prod. Appl. Clean Steels* **1972**, 186 (1972).
25. M. Hillert, H.Y. Lai, and G.X. Liu: *Alloy Diffusion and Thermodynamics* (Metallurgical Industry Press, Beijing, 1984).
26. Q.B. Li and X.C. Wang: *Diffusion Controlled Reaction and Thermodynamics in Alloys* (Liaoning Science and Technology Publishing House, 1984).
27. J. Xie, J.J. Yu, X.F. Sun, T. Jin, and Y. Sun: Carbide evolution behavior of K416B as-casting Ni-based superalloy with high W content during high temperature creep. *Acta Metall. Sin.* **51**(4), 458 (2015).
28. Z.C. Liu: *Metal Solid State Phase Transformation Tutorial* (Metallurgical Industry Press, Beijing, 2003).
29. S. Shanmugam, N.K. Ramiseti, R. Misra, T. Mannering, D. Panda, and S. Jansto: Effect of cooling rate on the microstructure and mechanical properties of Nb-microalloyed steels. *Mater. Sci. Eng., A* **460**, 335 (2007).